Analysis of Airborne Doppler Lidar Measurements of the Extended California Sea Breeze

JOHN J. CARROLL

Department of Land, Air and Water Resources, University of California, Davis, California

(Manuscript received 20 June 1988, in final form 29 March 1989)

ABSTRACT

The analysis of airborne Doppler lidar data taken by NASA near the top of the planetary boundary layer in the central valley of California is presented. These data include downward scan angles that intercept the ground. The maximum errors in the radial speeds, based on the apparent speed of the ground strikes, was found to have a magnitude of less than 2.0 m s^{-1}. These errors appear to have a slowly varying systematic part and a random part. The lidar radial speeds were corrected for running averages of these errors resulting in a random residual error of less than 0.3 m s^{-1} in magnitude.

Data are considered usable for those range bins in which the return signal amplitude exceeds that of the average shot noise by two times the rms variation in the noise. These data were analyzed to produce wind vectors on a geographic grid divided into 1 kilometer square cells. The resulting wind field appears to be very realistic and contains features similar to those apparent in ground level wind observations. The vertical shear in the sea breeze is well resolved as is its apparent containment below well-defined inversions.

While the analysis was labor intensive and cumbersome at this early stage of system development, the final product is a heretofore unattainable high resolution depiction of air flow over a broad region. The analyzed wind fields appear to be very realistic and easy to interpret. The technique is accurate in the sense that where the flow is slowly varying relative to the time sale of the measurement technique, the accuracy of the system is comparable to more standard techniques but with much greater spatial resolution than possible with other techniques. Where the flow is nonstationary, the recovered wind fields show this as well, i.e., the *variability* of the wind is correctly indicated. The success of this experiment is due to the high precision of the modified inertial navigation unit used and the use of ground strikes to provide absolute verification of total system performance.

1. Introduction

Measurements of the wind field associated with the intrusion of marine air into the central valley of California were made by personnel from the National Aeronautic and Space Administration (NASA) using their airborne Doppler lidar system following a flight path and scan pattern suggested by the author. The primary goal of this experiment was to demonstrate the utility of the method for the measurement of detailed wind fields at small space scales and to identify its limitations, if any. The extended sea breeze circulation is itself an interesting phenomena with important implications to the transport of air pollutants and to local microclimates (Fosberg and Schroeder 1966; Carroll and Baskett 1979). This method has the potential to reliably measure wind fields over several hundred square kilometers with spatial resolutions as small as 500 meters. These kinds of resolutions are very useful for verification of diagnostic and predictive models of local wind flows. The data analyzed were taken between 1400 and 1630 Pacific Daylight Time (PDT) on 27 August 1984.

Corresponding author address: Dr. John J. Carroll, Dept. of Land, Air and Water Resources, University of California, Davis, Hoagland Hall, Davis, CA 95616.

The airborne lidar system is described in Bilbro et al. (1984). It consists of a carbon dioxide laser (wavelength = 10.6 micrometers) which emits pulses in controllable directions. Radiation backscattered by small particles suspended in, and moving with, the air is collected by a telescope and focused on a detector. If the ensemble of scattering particles is moving with a component parallel to the emitted beam, the backscattered radiation will have a frequency differing from the source by an amount proportional to the speed of these particles relative to the laser. The system records the intensity and frequency shift of the returned signal. Using appropriate timing of the samples, these data can be obtained as a function of range. If a second beam crosses the first at a given range, the line-of-sight speed in that direction can also be measured and the speed and the direction of the flow in the plane of the two beams can be determined. Rather than use two lidars displaced in space, the airborne system uses the aircraft to move a single lidar allowing views of the same point in space from different directions offset in time. By removing the aircraft motion from the relative Doppler speeds, the movement of the air relative to the ground can be calculated.

For the flight reported here, the lidar was mounted on the left side of the aircraft and scanned approximately 20 degrees forward and back of the normal to

the flight path. Vertical angles of zero (horizontal) and −1, −2, −3, and −4 degrees (downward) were intended to be used. The horizontal scan pattern is illustrated in Fig. 1. Multiple pulses are emitted with the line of sight held constant (typically 40 to 100 pulses) and the information from all of these averaged to obtain the data in a given range bin for a particular "shot." With multiple pulse averaging, the true sample volumes are 300 meters long and between 20 and 300 meters wide. For the data analyzed here, the sample volumes are approximately 300 × 150 × 0.25 cubic meters. The data recorded for each range bin for each shot are, in order of increasing uncertainty, the average Doppler speed, the average intensity and the range in the Doppler frequencies among the multiple pulse returns.

In order to obtain the part of the radial Doppler speeds due to the air motion relative to the ground, the contribution of the aircraft motion must be removed. The accuracy of this calculation depends on the accuracy of the beam pointing angles and the accuracy of the recorded ground speed and ground track of the aircraft as well as the accuracy of the lidar system itself. Since the aircraft's speed is 10 to 20 times larger than typical wind speeds, the measurement errors are very sensitive to uncertainties in these variables. In earlier test flights, inaccuracies in the aircraft navigation and attitude data precluded successful recovery of meaningful wind fields. In later flights, an improved inertial navigation unit (INU) was used and negative elevation angles were included in the scan pattern to allow measurements of ground returns. From these, the apparent motion of the aircraft relative to the ground could be measured by the Doppler laser system itself. The ground return data form an internal means of assessing the total system's performance and the uncertainty in the radial wind components.

The wind vectors in the plane of the two beams can be calculated from the line-of-sight speeds and horizontal scan angles using

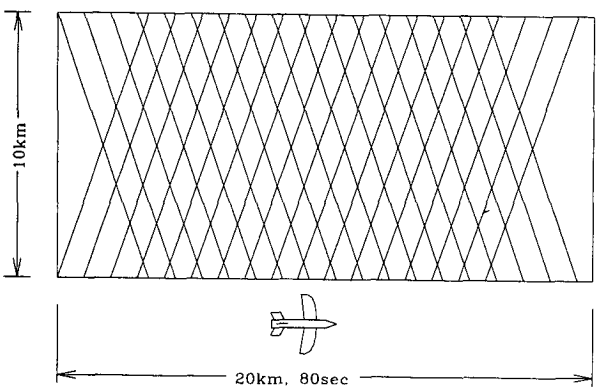

FIG. 1. Plan view of the sampling domain showing the airborne lidar scan pattern.

$$U_r = \frac{V_b - V_f}{\sin d_b + \sin d_f}$$

$$V_r = \frac{V_b + V_f}{\cos d_b + \cos d_f}. \quad (1)$$

These assume equal scan angles forward and back of the normal to the flight path.

Here V_b and V_f are the radial speeds in the backward and forward directions with the aircraft motion removed. Here, d_b and d_f are defined by

$$d_f = a_f + \frac{\pi}{2}$$

$$d_b = -\left(a_b + \frac{\pi}{2}\right) \quad (2)$$

with a_f and a_b being the scan angles measured relative to the line of flight; U_r and V_r represent the components of the wind parallel and normal to the flight track. These can then be converted to a wind speed and direction relative to the flight heading and rotated to geographic coordinates.

The accuracy of the wind so determined depends not only on the accuracy of V_b, V_f, a_f, and a_b but on whether the wind in the sample volume changed in the time between the forward and the backward sampling. An analysis of these effects on the accuracy of the recovered wind fields is contained in Carroll (1986). A major finding of that work is that if the real wind field contains variations on scales less than a few kilometers, the nonsimultaneous sampling inherent in this method results in recovered wind vectors that fail to represent the real wind in the sample volume at either the first or second sampling. In this situation the recovered vectors show a high degree of spatial variability. Although the recovered vectors do not represent the real vectors at the time and place of the measurement, they do, correctly, indicate that the flow is spatially varying and locally unsteady. Since the scans intersect at 40 rather than 90 degrees, the effect of these errors depends strongly on the mean wind direction relative to the flight path.

2. Experimental conditions

The area of study (Fig. 2) was chosen as it frequently contains an extended sea breeze circulation which has important implications to local air quality issues and has a variety of topographic features useful for testing diagnostic and predictive flow models. Of particular interest is the channeling of this flow through a gap in the coastal hills called the Carquinez Strait and the difluence of the flow into the Sacramento Valley to the north and the San Joaquin Valley to the south. There are also a number of vertical temperature soundings

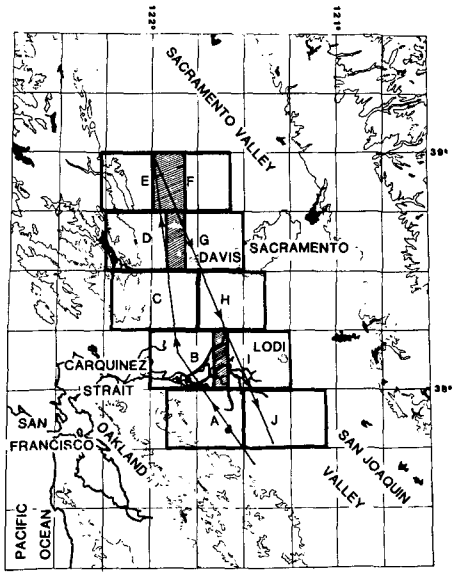

FIG. 2. Map of central California showing the aircraft flight track for the measurements taken 27 August 1984, 1400 to 1630 PDT. The regions A through J are the areas for which wind vectors are plotted. Each region is 15′ of latitude by 25′ of longitude. Topographic contour interval is 1000 ft.

taken in the area and a fairly dense network of hourly surface observing stations in the region.

Data were recorded for three circuits of the flight track shown in Fig. 2. These were flown at altitudes of approximately 760 meters (2500 ft) above mean sea level (MSL). Some systematic pointing errors were encountered, so that the actual vertical scan angles for which pairs of forward and backward scans overlap are approximately −1, −2 and −3 degrees.

The synoptic situation was dominated by a weak ridge aloft with an extremely flat pressure field. At 1700 PDT (0000 UTC) winds over Oakland were from 145 degrees at 10 m s^{-1} at 1500 meters and from 175 degrees at 5 mps at 1000 meters. Lowest inversions in the San Francisco Bay area and over the Carquinez Strait area were at or below 600 meters throughout the flight period. Further inland, at Davis and Sacramento, the midafternoon inversions were weaker and at altitudes of 800 meters or greater. With ridging aloft both to the north and south of the study area, the strength of the sea breeze intrusion was weaker than normal.

The local temperature and pressure fields analyzed for the times of the flight show that the pressure decreased inland, with the maximum horizontal pressure gradient being over the coastal mountains and especially in the Carquinez Strait area. The coolest temperatures are found along the coast at 18°C (65°F) in contrast to temperatures in excess of 35°C (95°F) inland. Surface wind observations for the same periods show a weak sea breeze intrusion with a typical splitting of the flow into the two arms of the central valley.

3. Lidar data analysis

Data from the flight were obtained from NASA on magnetic tape. Each record on the tape represents one shot and contains information on date, time, aircraft position and altitude, attitude, air speed, heading, horizontal and vertical scan angles, and a number of parameters describing laser performance and status. Also included are the raw Doppler velocity, average amplitude of the return (in db) and the frequency spread for each range bin from 1 to 95. These bins are centered 0.45 to about 30 Km from the aircraft respectively. These data were analyzed by making several passes over the records, each time creating a modified dataset until the final product was produced. The final product is a dataset gridded to geographic coordinates containing sets of forward and backward samples that lie within 500 meter square areas or cells centered on these coordinates. For each of these cells, the number of range bins falling within the cell is recorded, as are the corrected radial speeds, the relative amplitudes, the directions of the shots, the elevation angles, the coordinates of the range bins and the shot number from which the data were obtained.

The first phase of the analysis consisted of making a number of corrections and amendments to the raw data and reducing the total size of the records. A major concern is to establish at what range the return signal is so weak that the Doppler speeds are indeterminable. While data are recorded out to 95 range bins, useful returns were only received out to about 30 range bins. We chose the mean amplitude for range bins 76 to 95 to define the average noise level for each shot and computed the rms variation in signal amplitudes for these outer bins. After examining a large number of shots it appeared that the radial velocities were only reasonable if the signal amplitude exceeded the noise amplitude by twice the rms variation in the noise. The farthest range bin for which this was true defines the maximum range for which wind data can be recovered for that shot.

For those shots with negative elevation angles, the returns were searched for ground strikes. We define a ground return as one that has a relative amplitude at least 2.5 units higher than the next inner one and 10 units higher than the next outer one. Frequently, two ground returns were identified in a shot. Usually they were contiguous and both had near zero corrected Doppler speeds. Occasionally, however, hits were more than a kilometer apart. We believe this to be due to any of several causes. With the small elevation angles used, the beams have an almost glancing angle of incidence with the ground. Part of the beam may be intercepted by the top of a hill and the rest from the ground behind. Some of the radiation may be scattered by a "porous" object (e.g., a tree), with the remainder from the ground behind. Finally, since the shot is really

the average of an ensemble of shots spread horizontally, passing the edge of an obstacle would result in returns recorded in more than one range bin. We defined the closest ground return as that appropriate for evaluating total system performance. The index of the ground strike range bin was added to the header and the speed and amplitude from that range bin added to the data array.

The known systematic corrections were then made to the header and bin data. These include making an offset correction to the speed data in each good range bin and for the ground strike data. A set of corrections was provided by NASA (J. Rothermel, private communication) to the shot elevation angles. Finally, all range bins were searched for speeds greater than 15 mps. If such speeds were found, the data was flagged as bad by setting the relative amplitude negative. This check is necessary because occasionally the laser frequency "jumps," resulting in extreme and artificial Doppler shifts. This is also a problem in the innermost range bins as the detector is generally saturated immediately following the source pulse rendering the data in the first 3 to 6 range bins unreliable.

The corrected data and a reduced, corrected and amended version of its header were saved and the recorded Doppler speeds of the ground in the records with ground strikes examined. A sample of these is shown in Fig. 3. These speeds are in fact the errors in the radial speeds for the whole system, including instrument errors, uncertainties in the aircraft's motion and in the beam pointing angles. For all the data analyzed, these line-of-sight speed errors did not exceed 2.0 meters per second in magnitude and their short term running average varied slowly in time. We determined these errors as a function of time for the forward and backward shots and computed 2-minute running averages which were then subtracted from the data in each range bin of the shots centered in the time interval. With this procedure, the short term systematic errors were removed, leaving essentially random errors in the speeds with magnitudes of less than 0.3 mps and a mean value of zero.

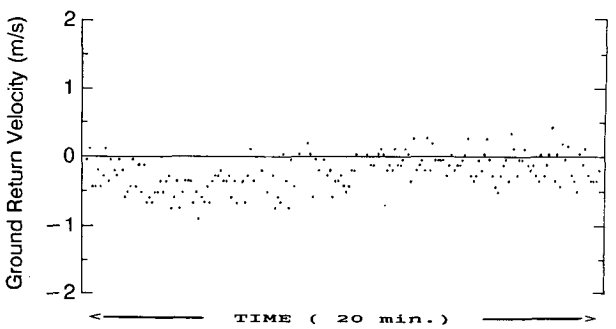

FIG. 3. Sample of ground return speeds as a function of time. Horizontal axis is time between 1537 and 1557 PDT.

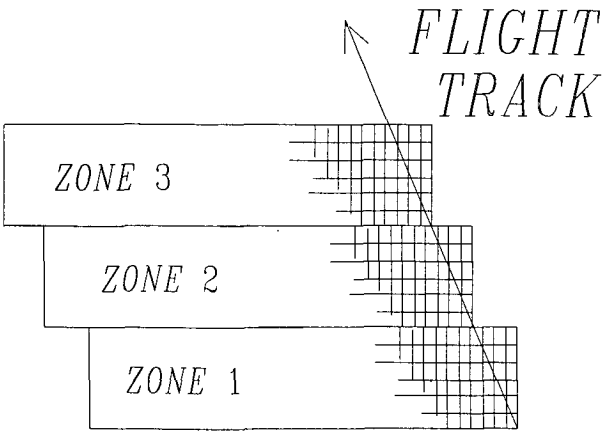

FIG. 4. Plan view of the relation of gridded zones and cells to the flight track.

The data were mapped onto a geographic grid of rectangular zones 3 km wide in the north–south direction and 18 km long in the west–east direction. A set of these zones and their relationship to a segment of the flight track is shown in Fig. 4. Each of these zones was subdivided into 500 × 500 meter square cells. The data from all "good" range bins that fall within each of these cells were then found. For each cell, these data are the number of range bins that fall in the cell and the relative amplitude, the corrected radial speed, geographic coordinates, horizontal and vertical scan angles and shot number for each range bin that lies within the cell. It is these data that are then used to calculate the wind vector for each cell.

In general, there was seldom more than one pair of forward and backward scan data with the same elevation angle in each cell. Often there would be two of one and only one of the other. Choosing the nearest neighbors, those with the highest amplitude or averaging like shots in calculating the wind vector for a cell made very little difference in the recovered wind. Shifting the coordinates of the zones, and thereby skewing which shots fell into different cells, also resulted in insignificant differences in the resulting wind field.

In the final phase of the analysis, we generated the wind fields for cells one kilometer on a side which in turn were mapped to the regions shown in Fig. 2. The resulting wind fields are shown in Figs. 5–10 for the second circuit of the flight track between 1443 and 1525 PDT. This part of the flight was chosen for detailed analysis because it had the most complete coverage and the fewest number of changes in the flight parameters and laser scan pattern. In these calculations there is no significant difference between choosing the pair of forward and backward shots closest to the center of the 1 km square, those with the highest amplitudes or averaging all of the like shots to compute the wind vector for the square. Given the fact that the vertical

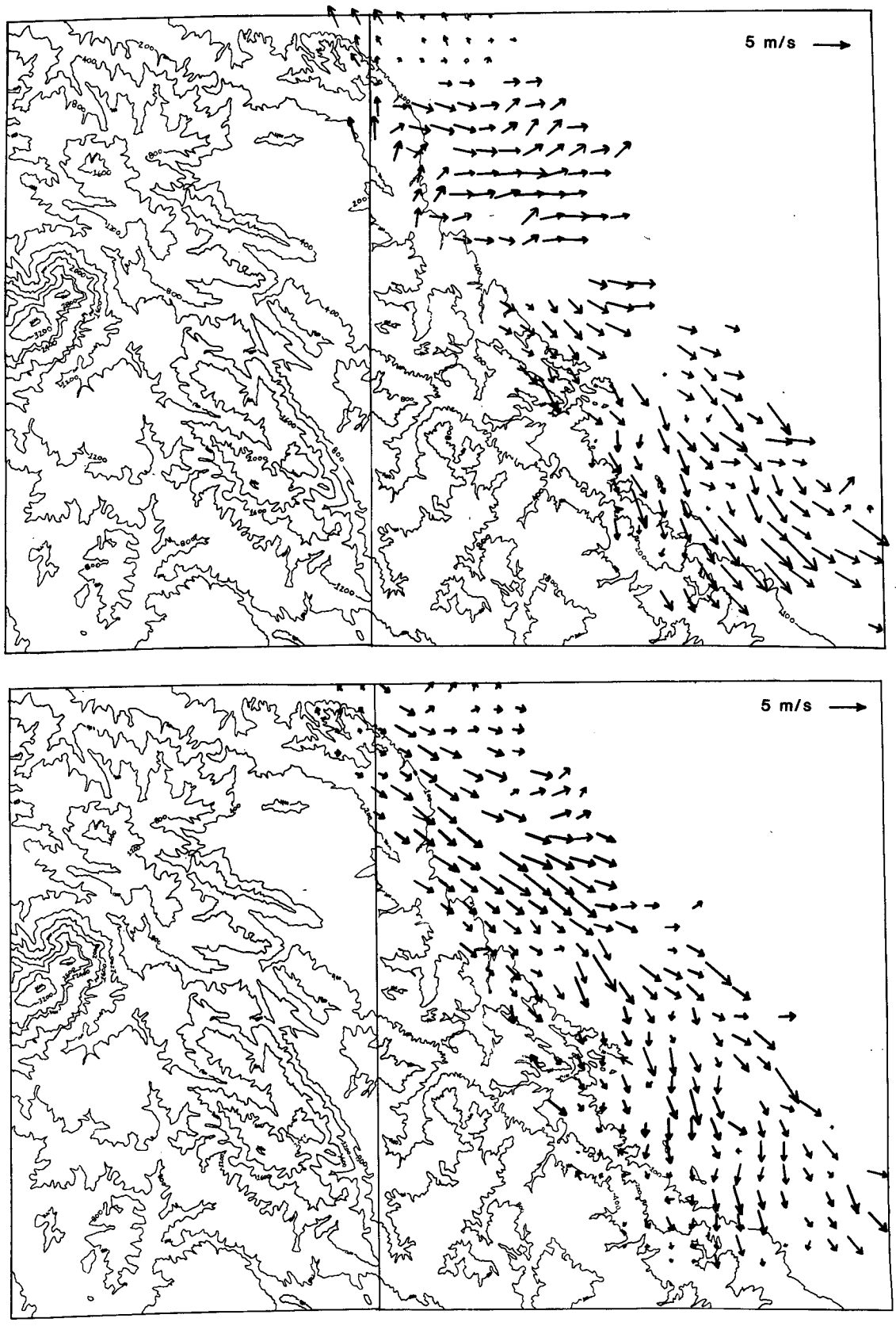

FIG. 5. Map of region A showing topography (contour lines are at 100, 200, 400 feet and at 400-foot intervals thereafter) and recovered wind vectors for elevation angles of (a) −1, and (b) −3 degrees from the horizontal.

angles of all of the forward shots appeared to be 0.3 degrees higher than the backward shots, greater sophistication in the horizontal spatial interpolation seemed unwarranted.

4. Results and interpretation

Several points should be kept in mind when examining the wind vectors in Figs. 5–10. The first is that the planes of the measurements are inclined downward to the left of the flight track. The vectors closest to the flight track are displaced 1 to 3 km from the aircraft and the farthest vectors are 10 to 15 km away. For a nominal elevation angle of −1 degree, the data are about 35 meters below the horizontal at a 2 km range and 210 m below at 12 km. For a nominal elevation angle of −3 degrees, the data are 105 and 630 m below the horizontal plane at 2 and 12 km respectively. The second point is that as the range increases, the time delay between forward and backward data from a given sample volume increases. If the resolved flows exhibit a high degree of spatial coherence, i.e., show a high degree of local organization and uniformity, then the variation of the wind within a sample volume between the forward and backward samples is small and the errors due to nonsimultaneous sampling are also small. This is the situation in the southern third of Fig. 6a, indicating that the recovered wind is a good representation of the true wind. If the recovered wind vectors exhibit a high degree of variability, as in the southern third of Fig. 5a, then the nonsimultaneous sampling errors are large and the plotted wind vectors do not represent the actual, instantaneous wind at either the time of the forward or of the backward sampling. The point is really moot, since a recovered field of this type means that the wind was in fact highly variable in the region and that is, in itself, useful information.

Figures 5 and 6 have several common features. The sea breeze intrusion appears to be relatively shallow in the vicinity of the strait, with a marked difference in the lidar detected flow at elevation angles of −1 and those detected with angles of −3. The flows aloft in the northern part of Fig. 5a and the southern part of Fig. 6a show southerly winds. Below these, the intrusion of the marine air appears as westerly winds which increase in strength with decreasing elevation. This flow is also marked by northwesterly winds along the east side of the hills in Fig. 5b. A temperature sounding taken at the time of the flight in this area shows a significant inversion at 540 m MSL or about 240 m below the aircraft altitude. This inversion most likely marks the top of the cooler marine air. For the scans with elevation angles of −1, this inversion lies below the plane of the lidar data at ranges less than 14 km. For elevation angles of −3, lidar data from ranges greater than 4.5 km are below this inversion.

Further north, comparable vertical wind shear is absent (Figs. 7 and 8). In this region the flow is basically from the southeast with some topographic channeling evident. At the lower elevations, the wind appears to turn to have a component upslope which may represent the buoyantly driven daytime slope flow. Inversion altitudes measured at this time at several locations in the Sacramento Valley near the flight path were greater than the aircraft altitude.

The flow farther east (Figs. 9 and 10) shows increasing organization of a northwesterly flow, characteristic of the sea breeze. Note that the degree of uniformity in the flow increases with decreasing altitude in this area, again indicating a relatively shallow intrusion. A temperature sounding, taken over Lodi one hour after the data shown in Fig. 9 were taken, showed a strong inversion based at the flight altitude.

5. Conclusions

The detailed wind fields derived from the lidar and conventional data appear to have a good correlation. The wind fields from the lidar data seem to have the same level of accuracy as those attainable by more conventional methods, such as pilot balloons and radiosondes. The lidar has the tremendous advantage of high density regional coverage.

In this study, data analysis procedures were cumbersome, time consuming and not amenable to real time analysis. With the experience gained from this and other studies using the airborne system, however, greater automation should be attainable in processing the data. In the present study, a great amount of time was spent in verifying the consistency between the header data and the range bin data and in determining the ground strike defined radial velocity corrections.

Although the elapsed time between intersecting views could be problematical, the delay times for these data were typically less than 90 seconds. Where the flow was spatially coherent, this delay was small relative to the local time rate of change of the wind; the recovered wind field appears to be valid. Where the wind was highly variable on this time scale, the recovered wind data showed a high degree of spatial variability that may not represent the real wind at any particular time but shows that the wind is, in fact, highly variable. The intermediate situation, in which the real wind and the recovered wind fields contain systematic variations such as vortex motions or wave motions on scales close to the scale of the analysis, is more difficult to interpret. If these structures are stationary in space, then the lidar should depict them accurately. If they are advected, their speed of translation compared to the delay time will determine how realistically the lidar derived wind field depicts the real wind field. This problem is particularly acute in the lowest layers in the atmosphere.

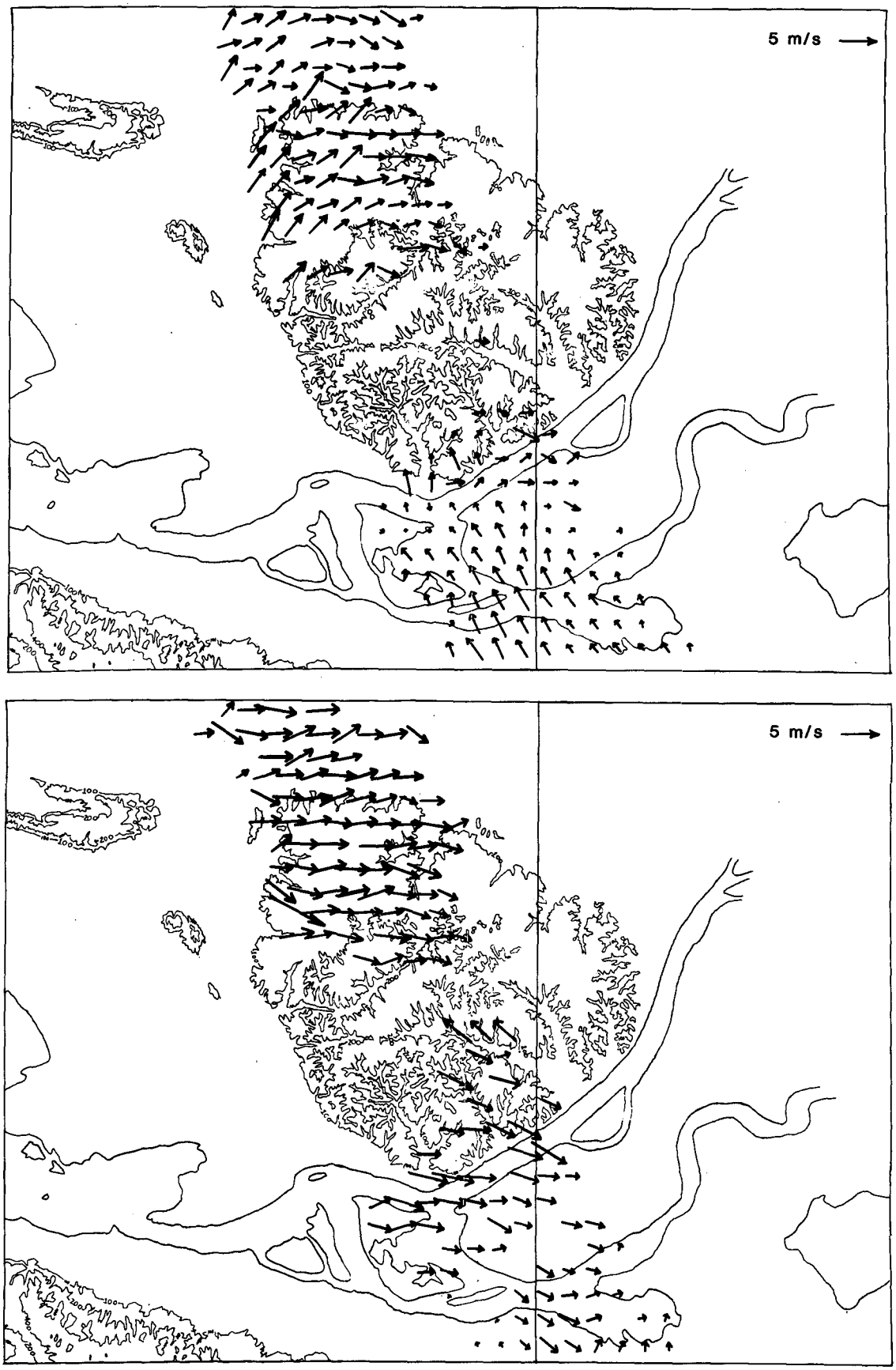

FIG. 6. As in Fig. 5 except for region B.

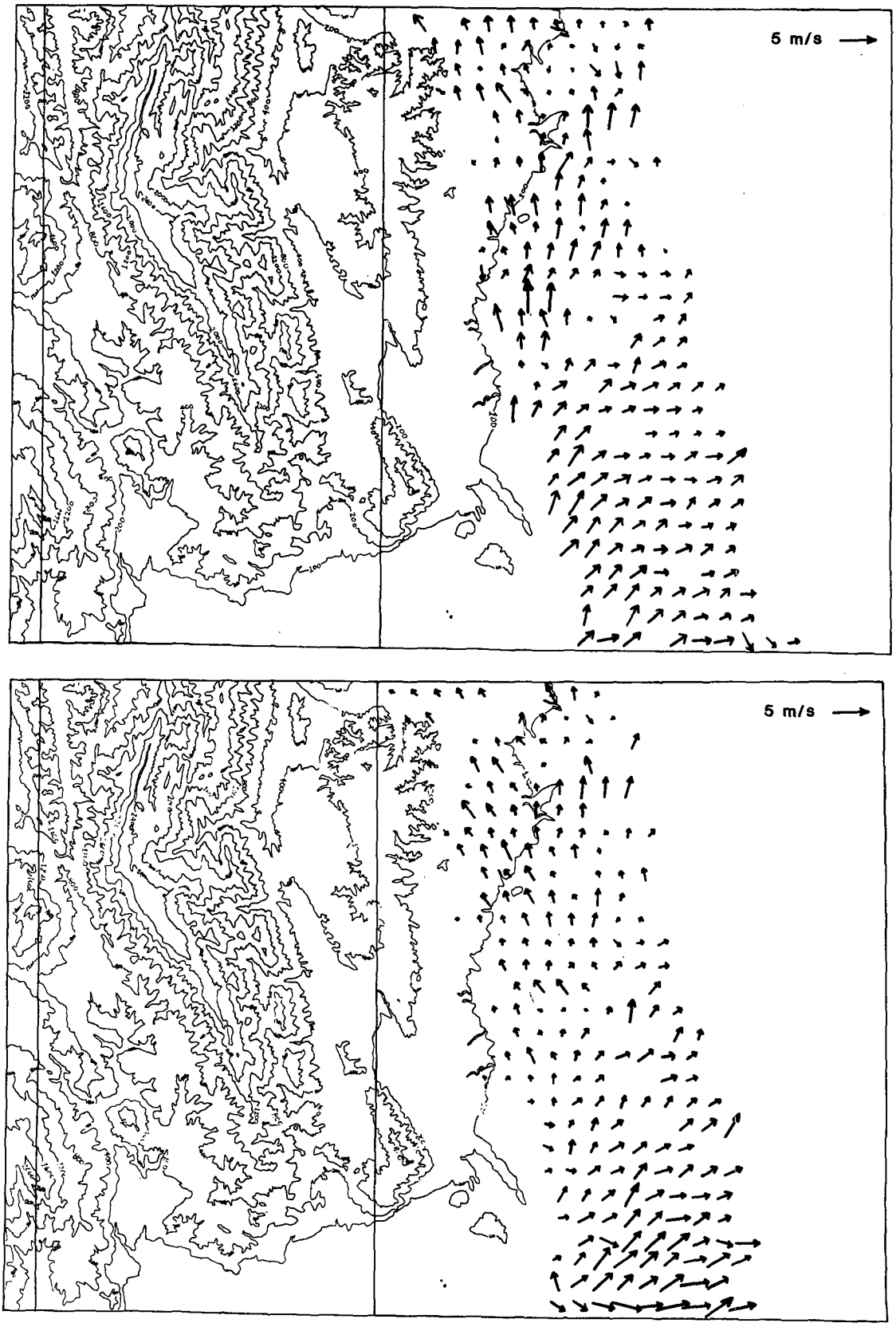

FIG. 7. As in Fig. 5 except for region C.

FIG. 8. As in Fig. 5 except for region D.

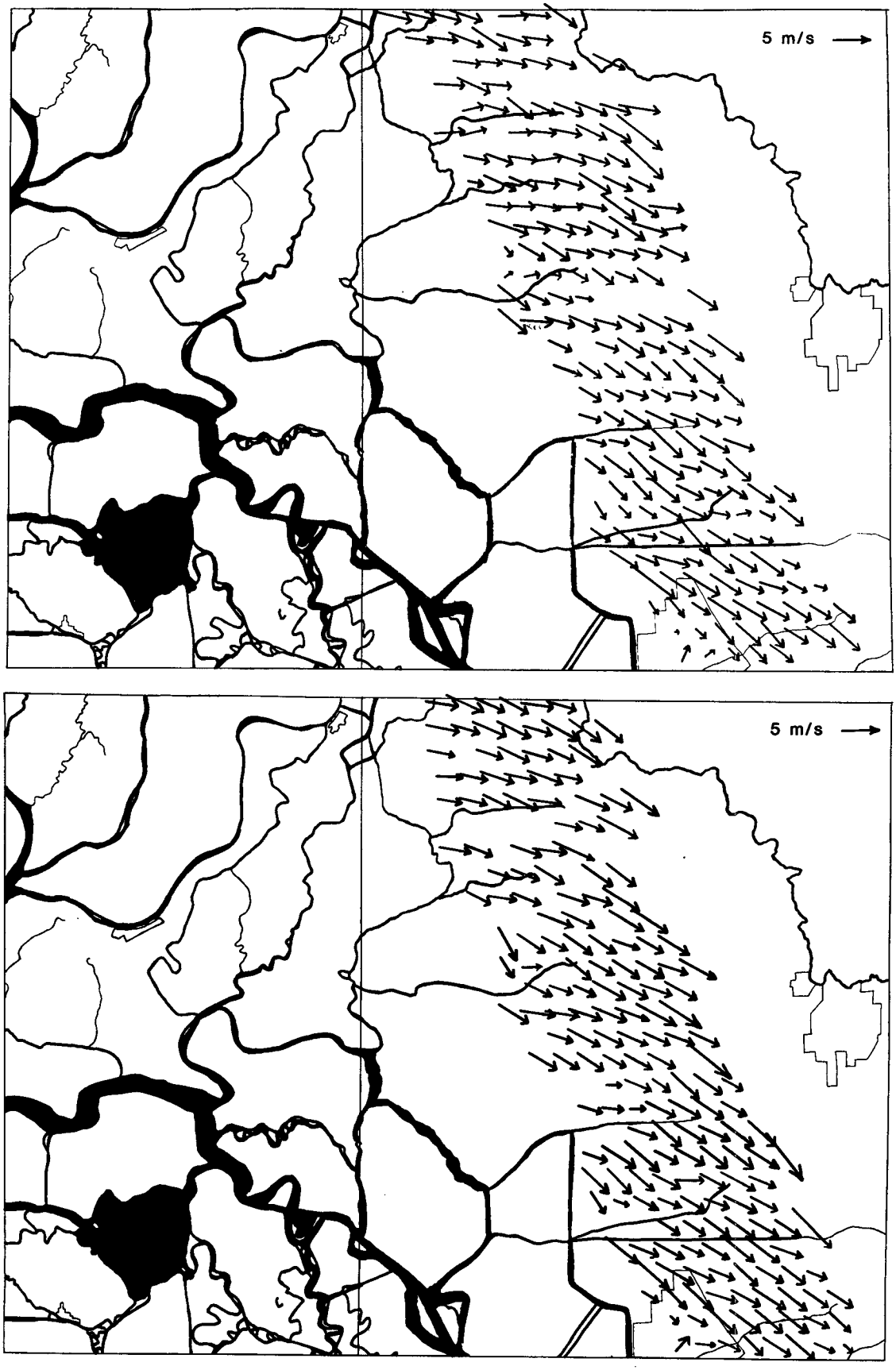

FIG. 9. As in Fig. 5 except for region I.

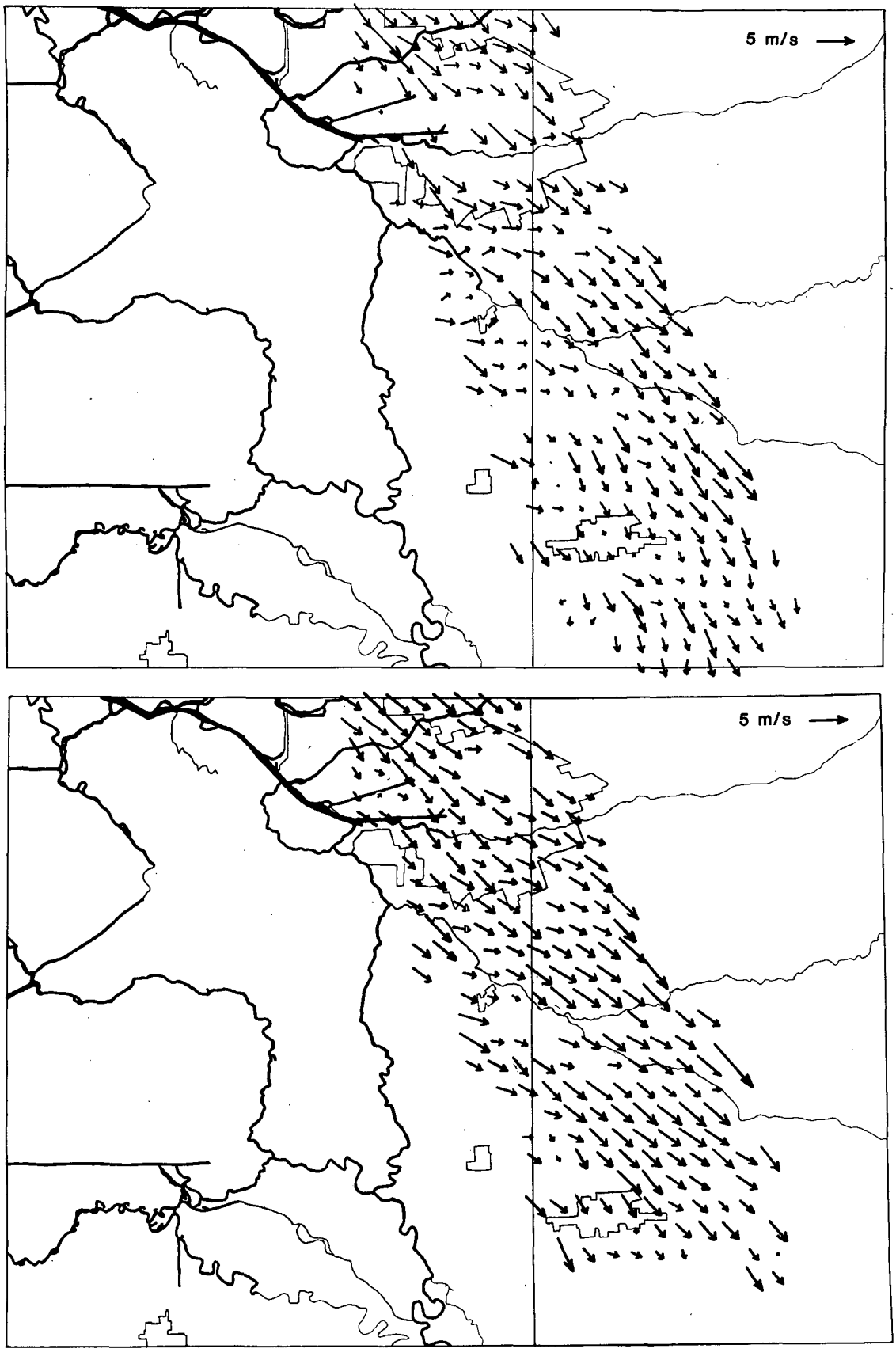

FIG. 10. As in Fig. 5 except for region J.

At altitudes above the boundary layer, the natural flow is much more coherent and measurements less sensitive to nonsimultaneous sampling.

Acknowledgments. Several students helped with the sometimes tedious and frustrating analysis of these data. Thomas McClellan, Luis Rodrequez-Mendez-Nunez, Loyal Brooks and Eric Russell contributed to the solution of one or more of these problems. The assistance of Dr. Jeffry Rothermel of MSFL was invaluable in sorting out apparent inconsistencies in the recorded data.

Support for this study was provided by NASA under contract NAS8-36550 and by the University of California, Agricultural Experiment Station.

REFERENCES

Bilbro, J., G. Fichtl, D. Fitzjarrald, M. Krause and R. Lee, 1984: Airborne Doppler wind measurements. *Bull. Amer. Meteor. Soc.*, **65,** 348–359.

Carroll, J. J., and R. L. Baskett, 1979: Dependence of air quality in a remote location on local and mesoscale transports: a case study. *J. Appl. Meteor.*, **18,** 474–486.

Carroll, J. J., 1986. Accuracy of wind measurements using an airborne Doppler lidar. *J. Atmos. Oceanic Technol.*, **3,** 3–11.

Fosberg, M. A., and M. J. Schroeder, 1966: Marine air penetration in central California. *J. Appl. Meteor.* **5,** 573–589.